Compaction of liquid immersed granular packings by small upward flows

Georges Gauthier and Philippe Gondret
Laboratoire FAST, Université Paris-Sud, CNRS, Université Paris-Saclay, F-91405 Orsay, France

(Received 19 July 2018; published 19 July 2019)

We study experimentally the compaction dynamics of a fully immersed granular packing subjected to a slow upward flow. We consider continuous flows as well as discontinuous flows featuring short flow bursts that act as flow "taps." We monitor the compaction rate of initial packings prepared by settling, and we find that compaction is possible for a continuous flow with upward velocities below the fluidization threshold. Flow bursts are found strongly to enhance the compaction efficiency, especially when the bursts are above the fluidization threshold.

DOI: 10.1103/PhysRevFluids.4.074308

I. INTRODUCTION

How identical spheres arrange in a dense packing is a long-standing scientific question that aroused many fundamental works since the famous Kepler conjecture: even if the solid fraction in the tetrahedral arrangement of four equal spheres in contact is 0.78, the highest solid fraction that can be achieved in a large packing is 0.74. This value corresponds to the densest periodic arrangement of equal spheres. In contrast, disordered packings correspond to much lower solid fractions. Random packings of equal spheres have a solid fraction of about 0.6 with a random loose packing limit (RLP) of about 0.56 and a random close packing (RCP) of about 0.64. For granular systems that are athermal and dissipative, the exploration of the different possible arrangements cannot be driven by temperature and must be driven by an external input of mechanical energy. This can be achieved by different modes of loading. The most classical way of compaction is the mechanical shaking of the container by successive taps [1–6] or harmonic vibrations [7]. The solid fraction first sharply increases, and then keeps increasing but more slowly toward a plateau. Two main empirical laws are used for describing the time evolution of the solid fraction from the initial packing value ϕ_0 to the final one ϕ_∞. The first law is expressed using a logarithmic time dependence, as [1,2]

$$\frac{\phi(t)-\phi_0}{\phi_\infty-\phi_0} = 1 - \frac{1}{1+B\ln(1+t/\tau)}, \tag{1}$$

where τ is a characteristic time of the compaction dynamics, and the parameter B is related to the compaction efficiency. The second law involves an exponential time dependence, as [1,3–5]

$$\frac{\phi(t)-\phi_0}{\phi_\infty-\phi_0} = 1 - e^{(-t/\tau)^\beta}, \tag{2}$$

involving a characteristic time τ and an exponent β related to the compaction efficiency.

The logarithmic evolution of Eq. (1) may be explained from simple theoretical arguments [8,9], e.g., by considering the process where a grain can jump into a hole only if the hole is large enough and by considering a distribution of hole sizes of Poisson type with a characteristic free volume [8]. The stretched exponential law is frequently used in a large range of relaxations of disordered thermal systems such as glasses [3]. The logarithmic evolution is experimentally observed for "confined" packings where the container-to-grain size ratio $D/2a$ is not very large ($D/2a \lesssim 10$), whereas the stretched exponential is observed for "unconfined" packings ($D/2a \gtrsim 10$). In the tapping

experiments of monodisperse spheres, the solid packing fraction typically increases from $\phi_0 \simeq 0.58$ to $0.61 \lesssim \phi_\infty \lesssim 0.63$. The characteristic time τ decreases with increasing levels of vibrations so that compaction is quicker for larger vibrations. By contrast, the final solid fraction ϕ_∞ decreases with increasing levels of vibrations so that compaction is higher for smaller vibrations [2,3]. Thus, an optimal way of compaction is to apply first large vibration levels for a first quick compaction before low vibration levels to achieve a final higher compaction up to about $\phi_\infty \simeq 0.65$.

Compaction has been shown also to be possible by shearing the granular packing from lateral wall deformation (e.g., [10,11]). This process appears to be quite efficient, with compaction ranging from $\phi_0 \simeq 0.59$ up to $0.66 \lesssim \phi_\infty \lesssim 0.69$ depending on the shear amplitude after a few 10^4 cycles typically. Such high values of solid fraction are beyond the RCP limit, and ordering is observed with some crystalline clusters at the walls but also in the bulk. In these shearing experiments, the compaction dynamics is complex and does not follow any of the model equations (1) and (2) mentioned above.

When grains are cohesive, the observed packing fractions are much lower, with reported values as low as 0.1, and display some compaction under vibrations by a two-stage process with two timescales, a short one and a large one, which are associated with collective and individual grain motions [12].

When the grains are fully immersed into a liquid, the bed packing that arises from settling depends on the hydrodynamic forces that come into play, which themselves depend on the particle Reynolds number and Stokes number [13,14], which compare fluid inertia and particle inertia, respectively, to viscous dissipation. Using fluidization/sedimentation cycles, Schröter *et al.* [15] studied the fluctuation statistics of the solid fraction of the obtained bed packings, which display small relative variations of about 0.1%. As for dry packings, compaction of liquid immersed granular packings can be achieved by taps [16] or harmonics vibrations [17]. In these compaction experiments where glass beads of about half a millimeter in diameter are immersed in a viscous liquid from one time to 1000 times the viscosity of water, the frequency is about the same ($\sim$50 Hz) and the maximal acceleration is about the same ($\sim 10g$, where g is the gravity acceleration), but the oscillation amplitudes are smaller than the grain size [17], whereas the tap amplitudes are larger than the grain size [16]. The solid fraction is observed to increase from about $\phi_0 \simeq 0.57$ [16] or 0.58 [17] up to $0.60 \lesssim \phi_\infty \lesssim 0.62$ [17] or $0.64 \lesssim \phi_\infty \lesssim 0.65$ [16], but the compaction dynamics is, however, more complex than in the dry case and cannot be given by the previous model equations (1) and (2). Indeed, a first quick dynamics followed by a second slow dynamics are observed, and the resulting dynamics has to be fitted by either a change in the exponent β of Eq. (2) [17] or by a change in the parameter B of Eq. (1) [16].

Despite all the previous reported studies, the compaction dynamics of granular packings is not fully understood. Yet the solid fraction of granular packings is a key parameter in numerous phenomena such as avalanches [18,19], impact cratering [20], or animal locomotion [21]. In some of these recent experiments, either air flow pulses [21] or a combination of continuous air flow and vibrations [19] are used to generate different compaction states.

In the present paper, we look at the possible compaction of liquid immersed granular packings by upward flows, which are either continuous or discontinuous with short flow bursts that act as flow "taps." In Sec. II, we present the experimental setup that allows us to prepare the initial packing from the settling of a fluidized bed before applying the upward flow. Then we show results for the compaction dynamics of the packing when submitted to a continuous flow below the fluidization threshold in Sec. III, and to successive short flow bursts in Sec. IV.

II. EXPERIMENTAL SETUP

The experimental setup is sketched in Fig. 1. Glass beads of radius $a = (1 \pm 0.05)$ mm and density $\rho_p = 2.3 \times 10^3$ kg/m^3 are dispersed in a water-glycerol mixture of 90% in mass of glycerol, with thus a density $\rho = 1235 \pm 1$ kg/m^3 and viscosity $\eta = (0.156 \pm 0.012)$ Pa s at $(24 \pm 1)\,^\circ$C. For the whole set of experiments, the total mass M_p of particles has been kept constant with the

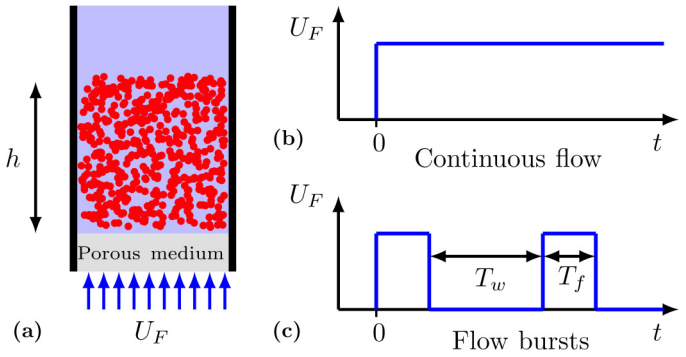

FIG. 1. (a) Sketch of the experimental setup. (b) Continuous flow with the constant upward velocity $U_F \neq 0$. (c) Bursting flow with the time period $T = T_w + T_f$ made of successive flow time T_f separated by nonflow time T_w.

value $M_p = 360 \pm 0.01$ g. The liquid immersed beads are contained in a vertical parallelepipedic cell 50 cm high and of rectangular cross section $S = 8 \times 2$ cm^2. The liquid is injected through a 2-cm-high porous medium located at the bottom of the cell and fitted with its rectangular section. The porous medium opening is 50 μm, with a permeability that is two orders of magnitude lower than the permeability of the granular bed. The upward volume flow rate Q is fixed using a gear pump allowing fluid circulation without any significant noise and dependence to pressure loss, which mainly comes from the porous media. The pump is controlled with a wave form generator that allows any requisite flow variations. For periodic bursts, we have checked that the flow rate in the cell is the one set, with no overshoot and very short time rise (smaller than 1/15 s) when the flow is turned on, and the same very quick response when the flow is turned off. We do not observe any mechanical disturbance when the flow is turned on or off. The experimental tank is lightened from behind and images of the cell are taken at the maximum rate of 15 images per second thanks to a camera located 1 m from the cell and with its axis horizontal and perpendicular to the largest side of the cell. The global solid volume fraction of the bed is measured through image analysis. From each individual image taken at time t, the bed surface is tracked and averaged spatially to obtain the mean instantaneous height $h(t)$ of the bed. We do not observe any significant curvature of the bed surface across the width and the thickness of the cell, rather we see a flat profile. The mean solid volume fraction $\phi(t)$ of the bed at time t is then deduced from $h(t)$ as $\phi(t) = M_p/\rho_p Sh(t)$, with an accuracy $\delta\phi/\phi = \delta h/h \simeq 10^{-3}$. Indeed in our experiments, the initial height value of the packing is about $h_0 \simeq 16$ cm for $\phi_0 \simeq 0.6$ and the accuracy of its measurement is $\delta h \simeq 0.1$ mm.

Considering the particles and the fluid used, the typical settling velocity of one isolated spherical particle is expected to be given by the Stokes velocity $U_s = 2(\rho_p - \rho)ga^2/9\eta \simeq 15$ mm/s corresponding to a viscous regime with a low particulate Reynolds $\mathrm{Re}_p = \rho U_s a/\eta \simeq 0.1$. The Stokes number corresponding to the ratio of particle inertia to viscous dissipation is $\mathrm{St} = 2\rho_p U_s a/9\eta \simeq 0.05$, thus very far below the critical value $\mathrm{St}_c \simeq 10$ corresponding to the bouncing transition [22,23]. This means that all kinetic energy is dissipated in the fluid in the grain contact process. In a low Re fluidized bed, the solid volume fraction ϕ is imposed by the upward flow velocity $U_F = Q/S$ according to the Richardson-Zaki (RZ) law, which reads [24,25] $\phi = 1 - (U_F/U_s)^{1/n}$. As shown in Fig. 2, our experimental data $\phi(U_F)$ agree fairly well with the RZ law with the exponent value $n \simeq 4.2$ and the experimental Stokes velocity $U_s \simeq 16$ mm/s close to the previously estimated value for a perfect monodisperse suspension of spheres.

Each initial granular pile is prepared following the same procedure. First, a fluidized suspension of solid fraction $\phi \simeq 0.22$ is obtained by imposing a constant upward velocity $U_F \simeq 5.7$ mm/s $\simeq 0.35U_s$. Then the upward flow is switched off and the suspension settles achieving a granular pile of solid fraction $\phi_0 = 0.605 \pm 0.005$. The critical fluidization velocity deduced from the RZ law

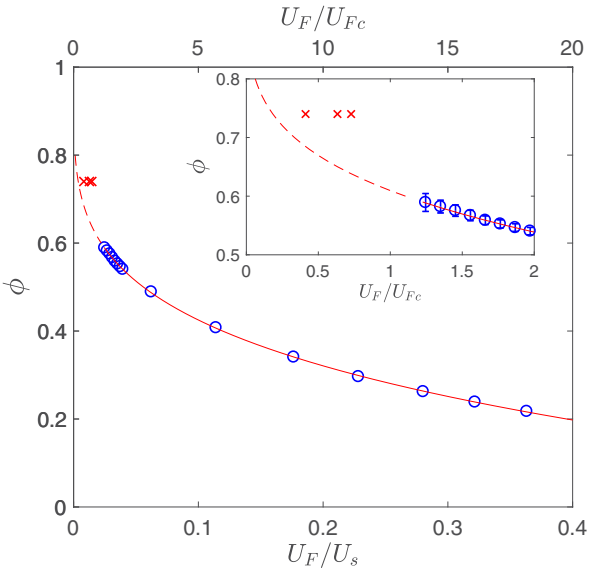

FIG. 2. Solid fraction of the granular bed ϕ as a function of the upward fluid velocity U_F normalized by the Stokes velocity U_s (bottom axis) or the critical fluidization velocity U_{Fc} (top axis). (○) Experimental data for fluidized beds above the fluidization threshold $U_{Fc}/U_s = 0.02$ and (—) best fit by RZ law $\phi = 1 - (U_F/U_s)^{1/n}$ with $n \simeq 4.2$ and $U_s \simeq 16$ mm/s. (×) Final value ϕ_∞ from best fit by Eq. (1) of $\phi(t)$ data of Fig. 3 corresponding to compaction experiments at $U_F < U_{Fc}$. Inset: zoom on flow range $U_F/U_{Fc} \leqslant 2$.

for beds of initial packing fraction $\phi_0 = 0.605 \pm 0.005$ is $U_{Fc} \simeq (0.02 \pm 0.001)U_s$. For $U_F > U_{Fc}$, the granular pile expands again toward a fluidized suspension of solid fraction $\phi < \phi_0$ according to the RZ law. In the following, we present experimental results for the compaction dynamics of the initial packing resulting from either a continuous flow [Fig. 1(b)] below the fluidization threshold ($U_F < U_{Fc}$) or successive flow bursts [Fig. 1(c)].

III. EXPERIMENTAL RESULTS

A. Continuous flow

Figure 3 displays the time evolution of the packing fraction $\phi(t)$ of the granular bed when normalized by its initial value ϕ_0 for three upward continuous flow velocities, $U_F/U_{Fc} = 0.4$, 0.6, and 0.7, below the fluidization threshold. In each case, ϕ increases with time with thus a compaction of the granular bed by the weak upward flow. This means that an upward continuous flow below the minimum of fluidization leads continuously to local rearrangements that result in an increase of the solid fraction ϕ. The compaction process is continuous during the long experiments that last typically a day, and no saturation that would lead to a final plateau value is seen. The compaction is higher for higher fluid velocity provided that the fluidization threshold is not overcome. For the highest possible flow rate $U_F/U_{Fc} = 0.7$, compaction is significant but rather slow as ϕ increases by about 2% after one minute (from 0.605 up to about 0.62), by about 4% after 1 h (up to $\phi \simeq 0.63$), and by about 6% (up to $\phi \simeq 0.645$) after 1 day. We have tested the two compaction laws reported in the Introduction and have found that the one based on a stretched exponential [Eq. (2)] does not fit well with our data, but the one based on a logarithm [Eq. (1)] does. This is not surprising as our system is rather confined with only 10 bead diameters in the smallest dimension [3]. For each data series, the best fit is found for the maximal possible volume fraction $\phi_\infty = 0.74$ but different values of the two other parameters B and τ. This means that in our compaction process, the predicted final packing is the highest achievable one, even if our highest measured solid fraction was

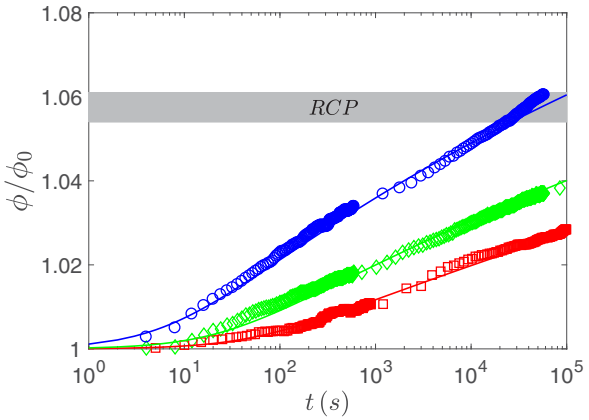

FIG. 3. Time evolution of the normalized solid fraction ϕ/ϕ_0 of the packing submitted to an upward continuous flow at three different velocities $U_F/U_{Fc} = 0.4$ (□), 0.6 (◊), and 0.7 (○) from an initial packing fraction $\phi_0 = 0.606$ (□), 0.607 (◊), and 0.603 (○). (—) Best fit by Eq. (1) with $\phi_\infty = 0.74$ and (□) $B = 0.019$ and $\tau = 55$ s, (◊) $B = 0.027$ and $\tau = 25$ s, (○) $B = 0.037$ and $\tau = 7$ s. The horizontal gray stripe corresponds to RCP.

$\phi \simeq 0.64$ for $U_F/U_{Fc} \simeq 0.7$ after one day. The RZ law by which the solid fraction is related to the upward velocity for a fluidized bed for $U_F > U_{Fc}$ seems thus no longer valid for a bed packing for $U_F < U_{Fc}$. The values of the compaction efficiency B and of the characteristic time of compaction τ when normalized by the characteristic settling time $a/U_{Fc} \simeq 3$ s are shown in Fig. 4 as a function of the dimensionless upward velocity U_F/U_{Fc}. For increasing U_F/U_{Fc}, B increases while τ decreases, which means that compaction is stronger and quicker for larger U_F/U_{Fc} provided that $U_F/U_{Fc} < 1$. Note that we do not observe any significant dependence of B and τ with ϕ_0. Note also that it was not possible to perform experiments below $U_F/U_{Fc} = 0.4$ because the pump does not deliver a continuous flow anymore at too low flow rates. In this limited flow range, the compaction time τ appears to decrease with increasing U_F and a linear fit of the data leads to a vanishing τ for $U_F/U_{Fc} = 0.85 \pm 0.15$, rather close to the value 1 corresponding to the experimental fluidization threshold. Note that at $U_F/U_{Fc} \simeq 0.9$, thus very close to the fluidization threshold, we observe some intermittency with successive irregular phases of compaction and decompaction. This behavior is not surprising and may be driven by some noise [26], and a similar intermittency with successives phases of mixing and segregation have been observed in fluidized beds with two grain sizes [27]. When the flow rate is significantly below the critical fluidization value ($U_F < 0.9U_{Fc}$), we think that compaction arises from packing inhomogeneities that lead to permeability inhomogeneities and thus to flow inhomogeneities: some local zones of lower packing fractions (higher permeabilities) are submitted to higher upward flow rates above the critical one that lead to local fluidization with possible local rearrangements.

B. Flow bursts

Let us now consider the effect of successive flow bursts. Our bursting experiments consist of a short flow time T_f followed by a long resting (no flow) T_w time before the next flow time, with thus the time period $T = T_f + T_w$ as sketched in Fig. 1(c). A constant upward velocity U_F is kept during each flow burst. The burst flow time T_f has been chosen such that the resulting fluid displacement is about one grain size, $T_f \sim a/U_F$, whereas the waiting time T_w has been chosen large enough for the grains to settle before the next flow burst, thus larger than the typical settling time $a/U_{Fc} \sim 3$ s. In practice, T_w is kept constant with the large enough value $T_w = 11$ s whereas T_f is adjusted with the U_F value in the range $0.5 \lesssim T_f \lesssim 4$ s. Figure 5 displays the time evolution of the normalized solid

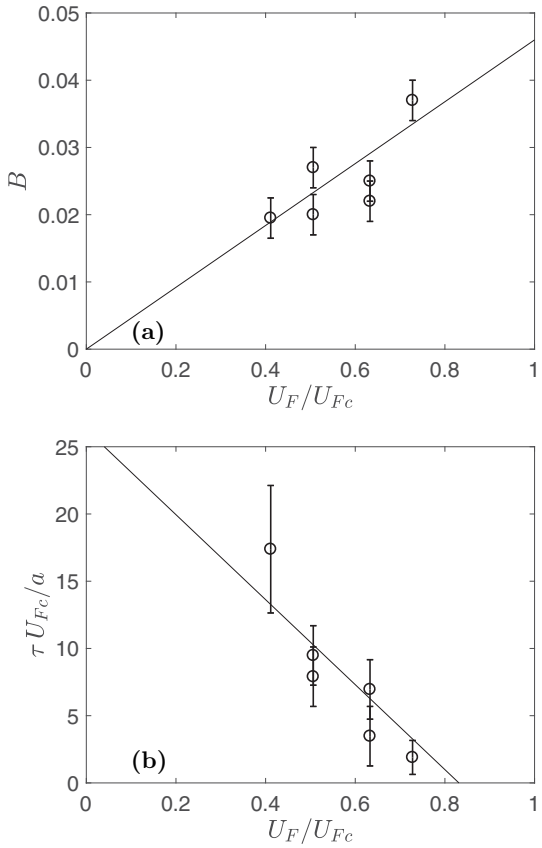

FIG. 4. (a) Amplitude B and (b) dimensionless characteristic time $\tau U_{Fc}/a$ of the compaction dynamics by upward continuous flow as a function of the dimensionless flow velocity U_F/U_{Fc}. (○) Experimental data and (—) best linear fits.

fraction $\phi(t)/\phi_0$ for two burst experiments with flow velocity below ($U_F/U_{Fc} = 0.4$) and above ($U_F/U_{Fc} = 2.6$) the critical fluidization velocity together with the continuous experiments of Fig. 3 corresponding to the same flow velocity below threshold. Two amazing facts arise from the results. The first amazing thing is that burst flow leads to a much more efficient compaction than continuous flow at the same value ($U_F/U_{Fc} = 0.4$) below the threshold of fluidization. Indeed, after one-day experiments corresponding here to about $N = t/T \simeq 6 \times 10^3$ flow bursts, the increase is of about 5%, whereas the increase is less than 3% by continuous flow. Burst flow is even more efficient for compaction when considering the injected fluid amount, which is reduced by the factor $T_f/T \simeq 0.27$ when compared to continuous flow. The second amazing thing is that compaction is still observed for flow bursts above the threshold of fluidization and that the resulting compaction is much more efficient than the one below. Indeed, after one day the compaction is of about 12% at $U_F/U_{Fc} = 2.6$ (see Fig. 5), thus 2.5 times higher than at $U_F/U_{Fc} = 0.4$. In that case, the bed solid fraction is observed to be above the random close packing value as $\phi_{\mathrm{RCP}} \simeq 0.64$ is reached after about only 4 min corresponding to only $N \simeq 20$ flow bursts, and $\phi \simeq 0.68$ is reached after about a one-day experiment ($N \simeq 7 \times 10^3$). At such a high solid fraction there should be some local crystallization as reported recently in compaction by periodic shear [11].

The detailed action of the flow bursts is shown in Fig. 6 where the time evolution of the top position of the packing h relative to its initial value h_0 and made dimensionless by the bead radius a, $(h - h_0)/a$, is plotted for a few first burst periods. When the burst flow velocity U_F is above

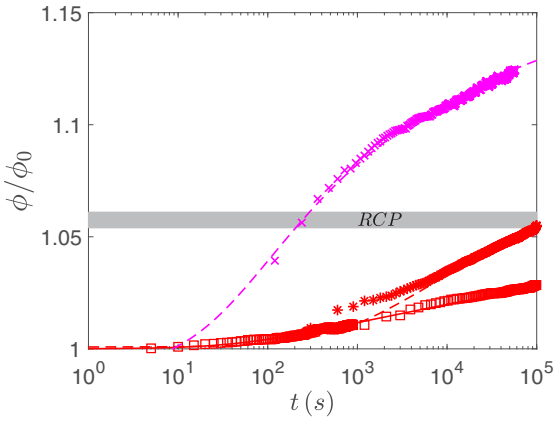

FIG. 5. Normalized solid fraction ϕ/ϕ_0 as a function of time t for upward flow bursts of dimensionless velocity (∗) $U_F/U_{Fc} = 0.4$ ($T = 15$ s) and (×) $U_F/U_{Fc} = 2.6$ ($T = 11,6$ s) corresponding to the same dimensionless flow displacement $T_f U_F/a = 0.54$ with accordingly varying burst time duration T_f, and the same waiting time $T_w = T - T_f = 11$ s. (- - -) Best fits by Eq. (1) with $\phi_\infty = 0.74$ and with (∗) $B = 0.07$ and $\tau = 945$ s, and (×) $B = 0.21$ and $\tau = 37$ s. (□) Same data and fit as in Fig. 3 for continuous flow at $U_F/U_{Fc} = 0.4$. The horizontal thick gray line corresponds to RCP.

the critical fluidization velocity U_{Fc}, the packing is slightly fluidized during each flow burst with a small decompaction of about $0.1a$ before a much larger compaction during the rest time T_w. By contrast, when the burst flow velocity is below the critical fluidization velocity ($U_F < U_{Fc}$), there is no fluidization as expected but a slow and almost continuous compaction.

By fitting the $\phi(t)$ data points of Fig. 5 obtained by flow bursts by the same logarithmic law as for continuous flows [Eq. (1)], we can extract the three parameters ϕ_∞, B, and τ. As for the packing compaction by a weak continuous flow, best fits of data series for burst flows lead always to the highest possible value for the ultimate solid fraction: $\phi_\infty = 0.74$. The values of the two other parameters B and τ when normalized by the typical settling time a/U_{Fc} are plotted in Fig. 7

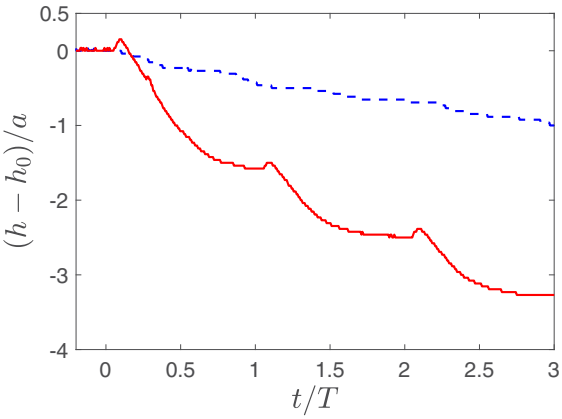

FIG. 6. Time evolution of the top position h of the packing relative to its initial value h_0 made dimensionless by the bead radius a during a few first flow bursts for a burst flow velocity U_F below (- - -), $U_F/U_{Fc} = 0.6$, $T_f/T = 0.26$ and above (—), $U_F/U_{Fc} = 2.6$, $T_f/T = 0.08$ the fluidization threshold U_{Fc}. The waiting time $T_w = 11$ s has been kept constant, whereas the flow time T_f has been varied to keep constant the fluid displacement $T_f U_F$.

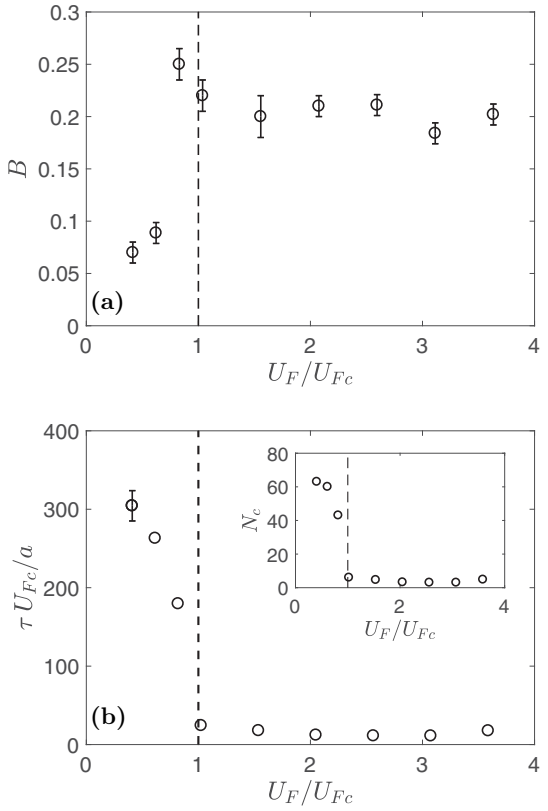

FIG. 7. (a) Compaction amplitude B and (b) dimensionless characteristic time $\tau U_{Fc}/a$ of the compaction dynamics as a function of the dimensionless flow velocity U_F/U_{Fc} with the same fluid displacement during flow burst $T_f U_F/a = 0.5$. Inset: Corresponding characteristic number of bursts $N_c = \tau U_{Fc}/a$ as a function of U_F/U_{Fc}.

as a function of the dimensionless burst flow velocity U_F/U_{Fc}. We observe that B increases and τ decreases when U_F increases below the critical fluidization velocity ($U_F/U_{Fc} < 1$) as for the continuous flow (Fig. 4). The B and τ values for compaction by flow bursts are, however, quite different from the ones by continuous flow. Indeed, B and $\tau U_{Fc}/a$ are about four times larger, but the effect of a larger B seems to be more important than the effect of a larger τ so that the compaction dynamics by flow bursts is larger than by continuous flow. Above the critical fluidization velocity ($U_F/U_{Fc} > 1$), the compaction efficiency parameter seems to saturate at a high plateau value $B \simeq 0.2$, whereas the characteristic time τ is very low ($\tau U_{Fc}/a < 3$). When looking at the characteristic number of bursts $N_c = \tau/T$ [see the inset of Fig. 6(b)], N_c decreases quite abruptly from about 60 when $U_F/U_{Fc} < 1$ to $N_c = 5 \pm 1$ when $U_F/U_{Fc} > 1$. This almost constant value may be due to the fact that the burst time T_f has been adjusted to the U_F value, e.g., the fluid displacement is the same and corresponds to about one grain size: $T_f \simeq a/U_F$.

IV. CONCLUSION

We have tested the possible compaction of liquid immersed granular packings, initially prepared by settling, from either continuous or bursting upward flow at low Reynolds number. The time evolution of the packing fraction was shown to follow a logarithmic evolution with three parameters corresponding to the ultimate solid packing, the compaction efficiency, and the characteristic time.

We have shown that compaction is possible with a continuous upward flow below the fluidization threshold, and that this compaction is stronger and faster close to this threshold. In this regime where the grains are no longer in suspension but form a dense packing with permanent contact, the usual law of Richardson and Zaki (RZ) that relates the solid fraction to the upward fluid velocity for fluidized suspensions seems no longer valid. Indeed, the observed logarithmic compaction process seems to go beyond the predicted RZ value for the solid fraction. A key point is that the compaction is even more efficient when the continuous flow is replaced by flow bursts. An even stronger and faster compaction is observed when the flow bursts are above the fluidization threshold, and this compaction seems to be the same when changing the flow rate but keeping constant the resulting fluid displacement for each burst flow. Complementary experiments should now be performed to explore the effect of the fluid displacement during each burst and to investigate the particle motions that lead to progressive compaction. An interesting point to investigate further would be the evolution of the packing state related to the different critical transitions [28] such as the glass transition, the jamming transition, and the intermediate Gardner transition [29] recently observed experimentally in granular media [30].

ACKNOWLEDGMENTS

We thank A. Aubertin, L. Auffray, and R. Pidoux for building the experimental setup, and A. Tariot for preliminary experiments. We acknowledge D. Salin, J. Martin, M. Nicolas, and M. Schröter for stimulating discussions. This work was supported by public grants from the French National Research Agency within the projects STABINGRAM (Grant No. 2010-BLAN-0927-01) and SSHEAR (Grant No. ANR-14-CE03-0011).

[1] J. B. Knight, C. G. Fandrich, C. N. Lau, H. M. Jaeger, and S. R. Nagel, Density relaxation in a vibrated granular material, Phys. Rev. E **51**, 3957 (1995).

[2] E. R. Nowak, J. B. Knight, E. Ben-Naim, H. M. Jaeger, and S. R. Nagel, Density fluctuations in vibrated granular materials, Phys. Rev. E **57**, 1971 (1998).

[3] P. Philippe and D. Bideau, Compaction dynamics of a granular medium under vertical tapping, Europhys. Lett. **60**, 677 (2002).

[4] P. Richard, M. Nicodemi, R. Delannay, P. Ribiere, and D. Bideau, Slow relaxation and compaction of granular systems, Nat. Mater. **4**, 121 (2005).

[5] P. Ribière, P. Richard, P. Philippe, D. Bideau, and R. Delannay, On the existence of stationary states during granular compaction, Eur. Phys. J. E **22**, 249 (2007).

[6] J. A. Dijksman and M. van Hecke, The role of tap duration for the steady-state density of vibrated granular media, Europhys. Lett. **88**, 44001 (2009).

[7] P. Richard, P. Philippe, F. Barbe, S. Bourlès, X. Thibault, and D. Bideau, Analysis by x-ray microtomography of a granular packing undergoing compaction, Phys. Rev. E **68**, 020301(R) (2003).

[8] T. Boutreux and P. G. de Gennes, Compaction of granular mixtures: a free volume model, Physica A **244**, 59 (1997).

[9] E. Ben-Naim, J. B. Knight, E. R. Nowak, H. M. Jaeger, and S. R. Nagel, Slow relaxation in granular compaction, Physica D **123**, 380 (1998).

[10] O. Pouliquen, M. Belzons, and M. Nicolas, Fluctuating Particle Motion during Shear Induced Granular Compaction, Phys. Rev. Lett. **91**, 014301 (2003).

[11] F. Rietz, C. Radin, H. L. Swinney, and M. Schröter, Nucleation in Sheared Granular Matter, Phys. Rev. Lett. **120**, 055701 (2018).

[12] J.-E. Mathonnet, P. Sornay, M. Nicolas, and B. Dalloz-Dubrujeaud, Compaction of noncohesive and cohesive granular materials under vibrations: Experiments and stochastic model, Phys. Rev. E **95**, 042904 (2017).

[13] G. Y. Onoda and E. G. Liniger, Random Loose Packings of Uniform Spheres and the Dilatancy Onset, Phys. Rev. Lett. **64**, 2727 (1990).
[14] G. R. Farrell, K. M. Martini, and N. Menon, Loose packings of frictional spheres, Soft Matter **6**, 2925 (2010).
[15] M. Schröter, D. I. Goldman, and H. L. Swinney, Stationary state volume fluctuations in a granular medium, Phys. Rev. E **71**, 030301(R) (2005).
[16] C. Lesaffre, V. Mineau, D. Picart, and H. Van Damme, Densification under vibration of a saturated granular packing, C. R. Acad. Sci., Ser. IV-Phys. **1**, 647 (2000).
[17] S. Kiesgen de Richter, C. Hanotin, P. Marchal, S. Leclerc, F. Demeurie, and N. Louvet, Vibration-induced compaction of granular suspensions, Eur. Phys. J. E **38**, 74 (2015).
[18] A. Amon, R. Bertoni, and J. Crassous, Experimental investigation of plastic deformations before a granular avalanche, Phys. Rev. E **87**, 012204 (2013).
[19] N. Gravish and D. I. Goldman, Effect of volume fraction on granular avalanche dynamics, Phys. Rev. E **90**, 032202 (2014).
[20] J. J. Soundar, N. Vandenberghe, and Y. Forterre, Unifying Impacts in Granular Matter from Quicksand to Cornstarch, Phys. Rev. Lett. **117**, 098003 (2016).
[21] C. Li, P. B. Umbanhowar, H. Komsuoglu, D. E. Koditschek, and D. I. Goldman, Sensitive dependence of the motion of a legged robot on granular media, Proc. Natl. Acad. Sci. (USA) **106**, 3029 (2009).
[22] G. G. Joseph, R. Zenit, M. L. Hunt, and A. M. Rosenwinkel, Particle-wall collisions in a viscous fluid, J. Fluid Mech. **433**, 329 (2001).
[23] P. Gondret, M. Lance, and L. Petit, Bouncing motion of spherical particles in fluids, Phys. Fluids **14**, 643 (2002).
[24] J. F. Richardson and W. N. Zaki, Sedimentation and fluidisation: Part I, Chem. Eng. Res. Des. **75**, S82 (1997).
[25] J. Martin, N. Rakotomala, and D. Salin, Accurate determination of the flux curve of concentrated suspensions, Phys. Fluids **7**, 2510 (1995).
[26] R. Fischer, P. Gondret, and M. Rabaud, Transition by Intermittency in Granular Matter: From Discontinuous Avalanches to Continuous Flow, Phys. Rev. Lett. **103**, 128002 (2009).
[27] A. Deboeuf, G. Gauthier, J. Martin, and D. Salin, Segregation and periodic mixing in a fluidized bidisperse suspension, New J. Phys. **13**, 075005 (2011).
[28] D. I. Goldman and H. L. Swinney, Signatures of Glass Formation in a Fluidized Bed of Hard Spheres, Phys. Rev. Lett. **96**, 145702 (2006).
[29] L. Berthier, P. Charbonneau, Y. Jin, G. Parisi, B. Seoane, and F. Zamponi, Growing timescales and lengthscales characterizing vibrations of amorphous solids, Proc. Natl. Acad. Sci. (USA) **113**, 8397 (2016).
[30] A. Seguin and O. Dauchot, Experimental Evidence of the Gardner Phase in a Granular Glass, Phys. Rev. Lett. **117**, 228001 (2016).